Part B

PROMISING EXPERIMENTAL TECHNIQUES

Chapter 4

Linear and Non-linear Optical Techniques to Probe Ion Profiles at the Air–Water Interface

Hubert Motschmann* and Patrick Koelsch†

Aqueous ions at interfaces play a substantial role in numerous processes in our environment. The diversity of ion-specific phenomena has been extensively investigated both theoretically and experimentally, and has expanded our knowledge about ion-specific effects. In particular, the *in situ* application of novel experimental tools such as non-linear optical spectroscopic techniques has led to a more detailed picture of interfacial ion profiles. Among these, second-harmonic-generation (SHG) spectroscopy and sum-frequency-generation (SFG) spectroscopy have emerged in recent years as suitable methods for characterizing aqueous interfaces. The selection rules for SHG and SFG dictate that a signal can only be generated in a non-centrosymmetric environment, effectively resulting in the suppression of isotropic bulk signal. This feature makes non-linear spectroscopy inherently surface-specific with submonolayer resolution, allowing for the tracking of subtle modifications in the interfacial layer. Being all optical techniques, SHG and SFG are also non-invasive and applicable under aqueous conditions, making them suitable for *in situ* characterization of ions at the air–water interface. In this chapter, an overview is given about linear and especially non-linear optical techniques used to investigate ions at charged and uncharged air–water interfaces. The theoretical background of non-linear optics is briefly reviewed and some recent experimental results are critically examined.

1. Introduction

Various manifestations of specific ion effects in physicochemical and biological systems have been discussed. For instance, the solubility of small

*Institute of Physical and Theoretical Chemistry, University of Regensburg, 93040 Regensburg, Germany.
†Institute of Toxicology and Genetics, Karlsruhe Institute of Technology (KIT), Hermann-von-Helmholtz-Platz 1, D-76344 Eggenstein-Leopoldshafen, Germany.

molecules such as benzene in aqueous solution depends strongly on the nature of the added salts as demonstrated in the work of McDevit *et al.*[1] All salting-in and salting-out effects are strongly influenced by the presence and the nature of the dissolved electrolytes. The solubility of proteins in aqueous solutions is governed by electrolytes in an ion specific fashion.[2] The catalytic activity of certain enzymes depends strongly on the nature of the salts. Pinna *et al.*[3] studied the hydrolytic activity of Aspergillus Niger Lipase and found that the activity is determined by the concentration and the nature of the dissolved electrolytes. The analysis of all these phenomena leads to the Hofmeister sequence of ions and its existence and widespread applicability suggests an underlying common principle.

Obviously, ions are not simple charged hard spheres. If so, ions with comparable diameter and valence should behave in a similar fashion, but that is not the case. However, why do ions act in a specific way? Are we able to identify a single parameter which can predict how a salt solution behaves in a certain experiment?

The answers which are discussed in this book are based on the following three concepts. The first one introduces ion specificity through collective dispersion type interactions; an ion specificity is thereby obtained by the explicit consideration of the size and the polarisability of the ions. Based on molecular dynamics (MD) simulation with polarisable force fields, Jungwirth and Tobias[4] state that induction interactions close to the free surface may be responsible for the preference of heavier ions at interfacial solvation sites. The asymmetric, incomplete solvation shell induces a sizable dipole on the anion at the interface, which is assumed to be the driving force for the interfacial propensity of the ions. MD simulation provides a very detailed picture of the interfacial architecture; however, the results depend strongly on the interaction potentials which are not exactly known. Hence, experiments are needed to verify the predictions. Indeed, this task is challenging and many sophisticated surface analytical techniques, even when pushed to the limits, may still yield only inconclusive results.

The second concept used for the interpretation of ion specificity focuses on the impact of the ion on the water structure. It is assumed that the ions distort the hydrogen bonding network leading to a particularly apt description of structure-breaking and structure-making ions. This should reflect the impact of the ions on the long range structuring of water. However, convincing experimental and theoretical evidence is missing. In contrary, there are strong experimental arguments against such a picture.

Smith *et al.*[5] analysed Raman spectra of water OH vibrations in potassium halide solutions. The spectral signature of the OH vibrational band is sensitive to details of the hydrogen-bonding network. Spectra of fluoride solutions are blue-shifted compared with neat water, whereas solutions of the heavier halides are red-shifted. These effects were previously explained in the framework of the structure-making and structure-breaking abilities. However, Monte Carlo simulations revealed that these perturbations are largely confined to the first solvation shell. Mancinelli *et al.*[6] identified further contradictions of the structure-maker/structure-breaker concept based on neutron diffraction study of NaCl and KCl solutions. Both cations are commonly classified as water structure-breakers, however, the analysis of the neutron diffraction experiment does not support this finding, instead pronounced differences in the solvation shell of both ions have been found. The sodium ions are more tightly solvated and more disruptive to water–water correlation as compared to potassium. So again, a suggestive picture is not really supported by experiments.

Last but not least, the idea of a specific chemical interaction has been proposed that leads to the formation of contact ion pairs, which is assumed to control the ion binding to proteins and their solubility. Kim Collins[7] introduces the law of matching water affinities that interprets the majority of ion specific effects, such as the formation of inner contact ion pairs. Here the driving force is not a specific chemical interaction between the oppositely charged ions; instead it is the consequence of the attractive force which is put in relation to the strength of the prevailing ion–water interaction. Small (hard) ions possess a tightly bound hydration shell, but the force between the ions is sufficiently strong to squeeze out the hydration shell. Big (soft) ions possess a loosely bound hydration shell, the electrostatic interaction is much weaker but still sufficiently strong to expel the hydration shell. The combination of hard and soft ions leads to a mismatch and both ions remain separated by a hydration layer. This simple concept has an amazingly predictive power.[7]

In this chapter, we focus on the simplest model system, namely the air–water interface, and its modification by the presence of ions. The major conceptual advantage is the simplification due to the absence of interfacial binding and the absence of ions in the gas phase. The reduced number of possibilities makes the air–water interface a crucial model system to study fundamental interactions. In a second step, complexity can be added by modifying the surface with a soluble or insoluble charged amphiphile,

allowing it to control the surface charge to a certain extent and to analyse the consequences experimentally.

Linear and non-linear optical techniques contribute to our understanding of the architecture of aqueous electrolytes–air interfaces. We discuss recent developments and accomplishment as well as the limitations and the underlying assumptions of these techniques.

2. Surface Tension Measurements

The conventional picture of the interface of simple aqueous salt solutions is based on thermodynamic analysis of the equilibrium surface tension isotherm. Valuable sources for the equilibrium surface tension isotherm of a simple aqueous electrolyte solution are the papers of Jarvis and Scheiman,[8] and P. Weissenborn and Robert J. Pugh (See Chap. 1, Fig. 8).[9]

In general, ions increase the surface tension in a specific manner. However, it is worth mentioning that certain combinations of ions decrease the surface tension or have a negligible effect on it. The thermodynamic analysis of the surface isotherm leads to the picture that the interfacial zone is depleted of ions. The surface deficiency is calculated using Gibbs equation as the derivative of the surface tension isotherm with a dividing plane chosen at a location that the surface excess of water vanishes.

$$\Gamma_{\mathrm{el}}^{\mathrm{H_2O}} = -\frac{1}{RT}\left(\frac{\mathrm{d}\gamma}{\mathrm{d}\ln a_{\mathrm{el}}}\right).$$

Here, γ is the equilibrium surface tension, a_{el} is the electrolyte activity and R is the gas constant and T denotes the temperature. Because of the fact that the slope of the isotherm is positive, it is concluded that the interfacial region is depleted of ions. This conclusion was further supported by a continuum dielectric model introduced by Onsager and Samaras,[10] suggesting that an ion is repelled from the interface between two media of different dielectric constant by an image charge of the same size and polarity located on the other side of the interface.

These observations and interpretations defined the textbook picture. This point of view has been challenged by the progress in understanding atmospheric reactions which in turn motivated molecular dynamics (MD) simulations.[4,11,12] MD simulations using polarisable force fields predict that soft ions such as halides are enriched at the interface with non-monotonic ion profiles. The book chapter of Pavel Jungwirth covers this in greater detail.

This is only an apparent contradiction to the conclusion drawn from the analysis of the equilibrium surface tension isotherm. Thermodynamics can accommodate several conflicting interfacial models provided that the integral excess or depletion is in accordance to Gibbs equation. Therefore, experiments are needed that yield direct insights in the interfacial architecture. These data can be obtained by optical techniques.

3. Challenges in the Investigation of Liquid–Air Interface

The investigation of aqueous electrolyte–air interface encounters a couple of intrinsic challenges. Firstly, the majority of material is dissolved in the bulk and the interfacial region comprises only a tiny fraction of the total material of the system. Consequently, spectroscopic investigations with classical techniques such as Infrared, Raman or UV-spectroscopy are often hampered by the lack of surface specificity and the signals are dominated by bulk contributions. Secondly, the processes at the air–water interface are highly dynamic. On a molecular scale there is a tremendous traffic towards both adjacent bulk phases. Molecules evaporate and condense at the interface and diffuse towards the bulk phase. There is no defined static molecular arrangement and as a consequence, fairly broad spectral features are expected. Moreover, many powerful surface specific techniques such as electron loss spectroscopy have special requirements to the sample and the environment (e.g. UHV-conditions) and cannot be applied to the liquid–air interface.

An elegant alternative which provides an intrinsic surface specificity is provided by non-linear optical reflection techniques based on a second-order effect (Fig. 1). Second-harmonic-generation (SHG) and sum-frequency-generation (SFG) spectroscopy contributed significantly to our current understanding of liquid–air, solid–liquid and liquid–liquid interfaces. Many fundamental insights on the structure of liquid–air interfaces are based on SHG and SFG experiments which are discussed in the next section.

3.1. *Basis of SHG and SFG Spectroscopy*

Second harmonic generation and sum-frequency generation have the same theoretical grounding outlined by Bloembergen and Pershan[13]. Shen

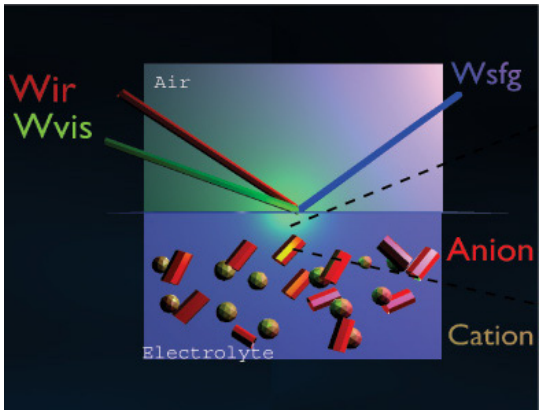

Fig. 1. Principle of an IR-VIS SF spectrum. (Reprinted with Permission from Ref. 63. Copyright 2007 American Chemical Society). The spatial and temporal overlap of an infrared and visible laser pulse at the interface generates light at the sum frequency which is emitted in a defined direction. A vibrational spectrum is obtained by scanning the infrared frequency. All second-order non-linear optical effects probe specifically the molecules at interfaces, and contributions from the bulk phase are to a large extent suppressed. *Note*. In an electrolyte solution, the majority of material is dissolved in the bulk and the interfacial region comprises only a tiny fraction of total material of the system.

et al.[14] were the first who recognised the potential as a surface specific probe in the mid-1990s.

SHG and SFG are the result of a non-linear polarisation wave that is generated by interacting ultrashort laser pulses at the interface of the two isotropic media: air and water. Both differ in the resonances probed. SHG results from the combination of two visible or near-infrared photons and probes the electronic states of the surface molecules. In an SFG experiment, two laser pulses are coincident in time and space at the interface of a sample. One visible laser pulse is fixed in frequency, while the other is tunable through the infrared region of 1000–3800 cm^{-1}. If the intensities of the incident laser pulses are sufficiently strong to induce a polarisation of the second order in the medium, an SFG signal oscillating at the sum-frequency of the two incident beams may be generated. If the frequency of the IR beam meets a frequency of a vibrational mode of the interfacial molecules, a resonance enhancement of the SFG signal may occur. To put it in simple terms, SFG spectroscopy provides a surface-specific vibrational spectrum while SHG probes the electronic signature of the molecules at the interface. Where does this interface specificity come from and what are the underlying assumptions?

The electric field propagating through a medium exerts a force on the valence electrons. The binding features of an electron can be described by a Morse type function. For small fields, the displacement of the electrons scales linearly with the applied field strength, while for stronger fields, deviations from the linear behaviour occur. Hence, the borderline between linear and non-linear optics is given by the binding potential of the electrons. Linear optics holds as long as the displacement of the electron occurs in a region where the binding potential can be approximated by a parabola. The induced dipole moment $\boldsymbol{\mu}$ can be represented as a power series of the electric field $\mathbf{E}$.

$$\boldsymbol{\mu} = \mu_0 + \alpha\mathbf{E} + \beta\mathbf{E}^2 + \gamma\mathbf{E}^3$$

The static dipole moment is denoted by μ_0, α is the linear polarisability of the electrons, β is the second order hyperpolarisability and so on. Non-linear optical effects are only noticeable once the electric field of the laser pulse is comparable to the inner-molecular fields.

The dominant term in the surface spectroscopy is the one of the second order, and the theory commonly used for the interpretation of SHG and SFG surface spectra is based on the electric dipole approximation. Within this approximation, the effect of optical magnetic fields and multipoles are neglected. This assumption can be at stake in some scenarios, especially for the interpretation of non-resonant SHG phenomena. Quadrupolar contributions are much weaker than the dipolar ones, but they scale with the number density and can amount to noticeable levels which may interfere with the surface term.[15–17] There is no general solution to this problem, and it is often not known *a priori* in SHG and SFG studies whether interfacial contribution is dominant over that of the bulk in an interface system.[18–20] Furthermore, it is commonly assumed that the dipoles induced in the molecules are solely due to the external laser field and that contribution from neighbouring molecules can be neglected. The local fields are hard to capture at a molecular level and require further theoretical work.[21] In this framework, the simplest description of SFG is given by

$$\mathbf{P}_{\mathrm{SF}}^{(2)} = \varepsilon_0 \chi^{(2)} \mathbf{E}_{\mathrm{VIS}} \mathbf{E}_{\mathrm{IR}},$$

where $\mathbf{P}_{\mathrm{SF}}^{(2)}$ is the second-order non-linear polarisation, ε_0 is the vacuum permittivity, $\chi^{(2)}$ is the second-order non-linear susceptibility, a third rank tensor describing the relationship between the incident electric fields vectors $\mathbf{E}_{\mathrm{VIS}}$ and $\mathbf{E}_{\mathrm{IR}}$ and the resultant polarisation. A simple symmetry consideration reveals that within the dipolar approximation, SHG or SFG

cannot occur within media with inversion symmetry. Inversion symmetry means $\mathbf{P}$ goes to $-\mathbf{P}$ if the direction of $\mathbf{E}$ is inverted, leading to vanishing polarisation response $\mathbf{P}^{(2)}$.

$$\mathbf{P} \stackrel{\text{i}}{=} -\mathbf{P} \quad \text{if } \mathbf{E} \stackrel{\text{i}}{=} -\mathbf{E}, \quad \text{hence } \mathbf{P}^{(2)} = \mathbf{0}.$$

In the framework of the dipole approximation, SHG or SFG cannot occur in isotropic bulk media such as fluids or gases. At the interface of two isotropic media, the symmetry is broken and the molecules possess a net orientational order reflecting the asymmetry of the environment. These molecules are probed by SHG and SFG leading to an interface specific response. It is important to realise that SHG or SFG *per se* does not provide information of the interfacial width without further assumptions. The signal is generated within the interfacial region and determined by the integral of the molecular orientational distribution function in between both bulk media.

The laboratory coordinate system is defined by the plane of incidence given by the beam direction and the normal of the reflecting surface. This is a distinct coordinate system since *p*- and *s*-polarisations are eigenpolarisations of an isotropic interface and furthermore, *p*- and *s*-lights do not interfere because of the mutual perpendicular orientation of the fields. The electric field vector is resolved in components parallel and perpendicular to the surface. Nevertheless, a variety of different axis systems and beam geometries are used in the literature and care must always be taken to relate equations derived for specific field directions and axis systems. A good overview is presented by Hirose *et al.*[22]

The reflectivity is given by the Fresnel factors that relate the reflected light E^r and transmitted light to the incoming field E^i as described in Ref. 23:

$$r_s = \left(\frac{E_s^r}{E_s^i}\right) = \frac{n_1 \cos\theta_1 - n_2 \cos\theta_2}{n_1 \cos\theta_1 + n_2 \cos\theta_2},$$

$$r_p = \left(\frac{E_p^r}{E_p^i}\right) = \frac{n_1 \cos\theta_1 - n_1 \cos\theta_2}{n_1 \cos\theta_2 + n_2 \cos\theta_2},$$

where n is the refractive index of media 1 or 2, and θ is the angle of incidence or refraction. The total electric field at the interface is given by the summation of the incident and reflected beam. The local electric fields at the surface drive a non-linear polarisation wave that is oscillating at the sum frequency in the case of SFG, or at twice the frequency of the incoming

light in the case of SHG. The resulting electromagnetic wave is coherently emitted in a direction given by momentum transfer. The SHG/SFG light is reflected and transmitted and the more accessible one is detected.

The non-linear susceptibility $\chi^{(2)}$ is a third-rank tensor comprising in total 27 elements; each one relates different combinations of the interacting field components to the induced non-linear polarisation. The generated polarisation wave is obtained by the summation of all different combinations and reads in the laboratory frame of reference:

$$P_{\mathrm{SF}}^{(2)} = \sum_{i}^{x,y,z} P_{i,\mathrm{SF}}^{(2)} = \varepsilon_0 \sum_{i}^{x,y,z} \sum_{j}^{x,y,z} \sum_{k}^{x,y,z} \chi_{ijk}^{(2)} E_{j,\mathrm{VIS}} E_{k,\mathrm{IR}}.$$

E is the surface field acting on the molecules which can be calculated by an evaluation of the Fresnel equations. It is common practice to transform the free propagating laser fields to the surface fields by the so-called K-factors:

$$K_x = \mp \frac{2n_{\mathrm{I}} \cos\theta_{\mathrm{I}} \cos\theta_{\mathrm{T}}}{n_{\mathrm{I}} \cos\theta_{\mathrm{T}} + n_{\mathrm{T}} \cos\theta_{\mathrm{I}}},$$

$$K_y = (1 + r_s) = \frac{2n_{\mathrm{I}} \cos\theta_{\mathrm{I}}}{n_{\mathrm{I}} \cos\theta_{\mathrm{I}} + n_{\mathrm{T}} \cos\theta_{\mathrm{T}}},$$

$$K_z = \sin\theta_{\mathrm{I}}(1 + r_p) = \frac{2n_{\mathrm{I}} \sin\theta_{\mathrm{I}} \cos\theta_{\mathrm{I}}}{n_{\mathrm{I}} \cos\theta_{\mathrm{T}} + n_{\mathrm{T}} \cos\theta_{\mathrm{I}}}.$$

The non-linear surface polarisation wave can be expressed in terms of the K-factors as

$$\mathbf{P}_{i,\mathrm{SF}}^{(2)} = \varepsilon_0 \chi_{ijk}^{(2)} K_j E_{p/s,\mathrm{VIS}}^{\mathrm{I}} K_k E_{p/s,\mathrm{IR}}^{\mathrm{I}}.$$

The relation between the polarisation wave and the emitted SFG radiation in the far field is provided by the so-called L-factors which are obtained by an evaluation of the continuity condition of the fields across the interface and the phase matching condition.

$$\mathbf{E}_{i,\mathrm{SF}} = L_i \mathbf{P}_{i,\mathrm{SF}}^{(2)},$$

$$L_x^{\mathrm{R}} = -\frac{i\omega_{\mathrm{SF}}}{c\varepsilon_0} \frac{\cos\theta_{\mathrm{SF}}^{\mathrm{T}}}{n_{\mathrm{T}} \cos\theta_{\mathrm{SF}}^{\mathrm{I}} + n_{\mathrm{I}} \cos\theta_{\mathrm{SF}}^{\mathrm{T}}},$$

$$L_y^{\mathrm{R}} = \frac{i\omega_{\mathrm{SF}}}{c\varepsilon_0} \frac{1}{n_{\mathrm{I}} \cos\theta_{\mathrm{SF}}^{\mathrm{I}} + n_{\mathrm{T}} \cos\theta_{\mathrm{SF}}^{\mathrm{T}}},$$

$$L_z^{\mathrm{R}} = \frac{i\omega_{\mathrm{SF}}}{c\varepsilon_0} \frac{(n_{\mathrm{T}}/n_{\mathrm{layer}})^2 \sin\theta_{\mathrm{SF}}^{\mathrm{T}}}{n_{\mathrm{I}} \cos\theta_{\mathrm{SF}}^{\mathrm{T}} + n_{\mathrm{T}} \cos\theta_{\mathrm{SF}}^{\mathrm{I}}}.$$

Experimentally, the intensity of the *s*- or *p*-polarised SF light is detected. For *p*-polarisation, it reads:

$$\begin{aligned} I_{p,\mathrm{SF}} &\propto |\mathbf{E}_{x,\mathrm{SF}}|^2 + |\mathbf{E}_{z,\mathrm{SF}}|^2 \\ &\propto |L_x \mathbf{P}^{(2)}_{x,\mathrm{SF}}|^2 + |L_z \mathbf{P}^{(2)}_{z,\mathrm{SF}}|^2 \\ &\propto \left| L_x \sum_j^{x,y,z} \sum_k^{x,y,z} \varepsilon_0 \chi^{(2)}_{xjk} K_j E^{\mathrm{I}}_{\mathrm{VIS}} K_k E^{\mathrm{I}}_{\mathrm{IR}} \right|^2 \\ &\quad + \left| L_z \sum_j^{x,y,z} \sum_k^{x,y,z} \varepsilon_0 \chi^{(2)}_{zjk} K_j E^{\mathrm{I}}_{\mathrm{VIS}} K_k E^{\mathrm{I}}_{\mathrm{IR}} \right|^2 . \end{aligned}$$

The decisive information is contained in the second-order non-linear susceptibility. The oriented gas model relates the macroscopic quantity susceptibility $\chi^{(2)}$ to the microscopic hyperpolarisability β. Subject to certain simplifying assumptions, it states that the susceptibility is given by the summation of all hyperpolarisabilities of all molecules. The underlying assumptions have been assessed in Ref. 24 and found to be valid.

Both tensors are described in a different frame of reference: the $\chi^{(2)}$ tensor is given in the laboratory frame of reference based on the plane of incidence, whereas the hyperpolarisability tensor in the molecular frame of reference defined by the symmetry of the molecule. An Euler transform relates both, leading to rather lengthy expressions between the corresponding tensor components, which are best handled and manipulated with the aid of a symbolic programming language such as Maple or Mathematica.

$$\begin{aligned} \beta_{IJK} &= \mathbf{U}_{Ii}(\phi,\theta,\psi)\beta_{ijk}\mathbf{U}^{-1}_{Jj}(\phi,\theta,\psi)\mathbf{U}^{-1}_{Kk}(\phi,\theta,\psi), \\ \mathbf{U} &= \mathbf{R}_c\mathbf{R}_b\mathbf{R}_a, \\ R_c(\psi) &= \begin{pmatrix} \cos\psi & \sin\psi & 0 \\ -\sin\psi & \cos\psi & 0 \\ 0 & 0 & 1 \end{pmatrix}, \\ R_b(\phi) &= \begin{pmatrix} \cos\phi & \sin\phi & 0 \\ -\sin\phi & \cos\phi & 0 \\ 0 & 0 & 1 \end{pmatrix}, \\ R_a(\theta) &= \begin{pmatrix} \cos\theta & 0 & -\sin\theta \\ 0 & 1 & 0 \\ \sin\theta & 0 & \cos\theta \end{pmatrix}. \end{aligned}$$

The individual tensor components are given by an orientational average of the adsorbed molecules within a volume defined by the coherence length of the incident light. The non-linear susceptibility $\chi^{(2)}$ contains information about the number density N and the orientational average of the molecules.

$$\chi^{(2)}_{ijk} = \frac{N \sum_{\alpha\beta\gamma} \langle R(\psi)R(\theta)R(\phi)\beta_{\alpha\beta\gamma}\rangle}{\varepsilon_0(\omega_\upsilon - \omega_{\mathrm{IR}} - i\Gamma)},$$

where ω_{IR} is the frequency of the incident infrared light, ω_υ is the eigen-
where ω_{IR} is the frequency of the incident infrared light, ω_υ is the eigen-
frequency of a vibrational mode and Γ^{-1} is the relaxation time of the vibrationally excited states in the resonance. A further analysis requires assumptions about the prevailing orientational distribution function. In the majority of studies, a narrow Gaussian or δ-shaped orientational distribution is assumed for the sake of simplicity.

Vibrational modes can only be excited in an SFG experiment if they are simultaneously infrared and Raman active. The hyperpolarisability reads

$$\beta_{\alpha\beta\gamma} = \frac{1}{2\hbar}\frac{M_{\alpha\beta}A_\gamma}{\omega_\upsilon - \omega_{\mathrm{IR}} - i\Gamma},$$

where $\hbar$ is the reduced Planck constant, $M_{\alpha\beta}$ and A_γ are the Raman and infrared transition moments.

$$M_{\alpha\beta} = \sum_s \left[\frac{\langle g|\mu_\alpha|s\rangle\langle s|\mu_\beta|\upsilon\rangle}{\hbar(\omega_{\mathrm{SF}} - \omega_{sg})} - \frac{\langle g|\mu_\beta|s\rangle\langle s|\mu_\alpha|\upsilon\rangle}{\hbar(\omega_{\mathrm{VIS}} + \omega_{sg})}\right],$$

$$A_\gamma = \langle \upsilon|\mu_\gamma|g\rangle.$$

μ is the electric dipole operator, g denotes the ground state and υ the excited state, and s refers to any intermediate state.

In an SFG experiment, the frequency of the incoming infrared light is changed. A resonance enhancement occurs if the infrared frequency matches the frequency of the vibrational mode leading to a resonant SFG signal. The frequency dependence of the non-linear susceptibility component can be split into a real and an imaginary part leading to

$$\chi_{\mathrm{R}} \propto \frac{1}{\omega_\upsilon - \omega_{\mathrm{IR}} - i\Gamma} = \frac{\omega_\upsilon - \omega_{\mathrm{IR}}}{(\omega_\upsilon - \omega_{\mathrm{IR}})^2 + \Gamma^2} + i\frac{\Gamma}{(\omega_\upsilon - \omega_{\mathrm{IR}})^2 + \Gamma^2}.$$

Beside the resonant part χ_{R}, there is also a non-resonant part χ_{NR} to the non-linear susceptibility which further complicates the analysis. The measured SFG signal is given by the interference between both:

$$\chi^{(2)} = \chi^{(2)}_{\mathrm{R}} + \chi^{(2)}_{\mathrm{NR}},$$

$$I_{\mathrm{SF}} \propto ||\chi^{(2)}_{\mathrm{R},ijk}|e^{i\delta} + |\chi^{(2)}_{\mathrm{NR},ijk}|e^{i\varepsilon}|^2,$$

with the phases δ and ε. At the air–water interface, the non-resonant part is usually fitted to a single value and phase, and the resonant part is described by assuming discrete resonances. In the case of metallic or semi-conductor supports, the line shape and the signal strength is determined by the interference between resonant and non-resonant parts. In any case, SFG analysis must occur after a deconvolution in component peaks. A direct comparison of the raw spectra to Raman- or IR-spectra may be misleading because of interference effects. This theoretical framework outlines the modelling strategy for fitting the spectra.

SFG spectroscopy is the only spectroscopy capable of producing vibrational water spectra of the air–water interface. The analysis is simplified by the symmetry of the interface and the symmetry of the molecule which reduces the number of independent tensor elements of the hyperpolarisability. The water molecule belongs to the point group $C2\mathrm{v}$ and the number of independent tensor elements is reduced to five: β_{caa}, β_{aca}, β_{aac}, β_{bbc}, and β_{ccc}. Of these, only β_{bbc}, β_{aac}, and β_{ccc} are non-zero for the symmetric stretch and β_{caa} and β_{aca} are non-zero for the anti-symmetric stretch. We denote the tilt angle between the molecular $C2$ axis and the surface normal Θ and ψ as the twist angle of the molecular plane with respect to the surface plane. Then, the relationship between the molecular hyperpolarisability, and the macroscopic hyperpolarisability, for the symmetric stretch after Euler angle transformations yields:

$$\chi_{xxz} = \chi_{yyz} = \frac{N_s}{2}\beta_{ccc}[(r+1)\langle\cos\theta\rangle - (1-r)\langle\cos^3\theta\rangle]$$

$$\chi_{xzx} = \chi_{yzy} = \chi_{zxx} = \chi_{zyy} = \frac{N_s}{2}\beta_{ccc}(\langle\cos\theta\rangle - \langle\cos^3\theta\rangle)(1-r)$$

$$\chi_{zzz} N_s\beta_{ccc}[r\langle\cos\theta\rangle + (1-r)\langle\cos^3\theta\rangle]$$

This framework outlines the underlying complexity in analysing SFG spectra.

3.2. *Experimental Setups*

Picosecond (ps) and femtosecond (fs) laser systems are most often used for SFG spectroscopy. Ps SFG spectrometers cover a wide spectral scanning range (about 1000 cm^{-1} without realignment). The narrow band ps light pulses are tuned through the spectral region, while the SFG signal is generally collected for a few minutes for each wave number to gain reasonable S/N ratios (the repetition rate for ps light pulses is usually in the order of 10–25 Hz). Detecting spectral regions of about 1000 cm^{-1} usually takes several tens of minutes. In this setup, the advantage of a wide scanning range is offset by the difficulty of performing time-dependent experiments.

Broadband SFG spectroscopy is based on fs laser pulses (usually around 120 fs) covering a spectral range of about 200 cm^{-1}.[25–29] The repetition rate of these systems is two orders of magnitude higher compared to ps systems (of the order of 1 kHz). This allows around 1000 acquisitions per second in a spectral range of about 200 cm^{-1}, with a reasonable S/N ratio in about 2–5 minutes. In a fs SFG spectrometer, a narrow band ps visible pulse is mixed at the interface with a broadband fs infrared pulse. The resulting broadband SFG signal is dispersed on a grating within a spectrometer and subsequently imaged by an intensified or backlight illuminated CCD camera.

3.3. *SFG and SHG Measurements at the Air–Water Interface*

The SFG spectra of the air–water interface measured in different laboratories with many different instrumentations agree reasonably well.[30–34] A typical spectrum of water in *ssp* polarisation is presented in Fig. 2. The first letter *s* denotes the polarisation of the SFG light, the second letter *s* refers to the one of the visible light and the last letter refers to the polarisation of the IR radiation which is set to *p*.

The spectrum shows a broad band in the 3000–3600 cm^{-1} region which is attributed to hydrogen bonded water and a narrow peak at 3700 cm^{-1}. Water is stabilised by the formation of a tetrahedral hydrogen bonding network. At the surface, this network is necessarily distorted leading to water molecules that cannot fully participate in the hydrogen bonding network and possess a non-hydrogen bonded OH. There is broad consensus within the scientific community about the nature of

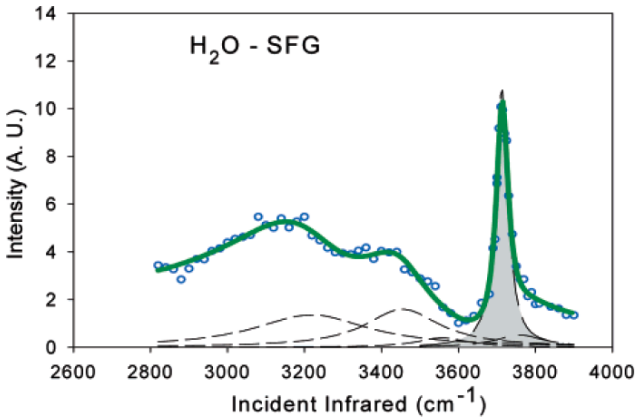

Fig. 2. SSP–polarised spectrum of neat water in the O–H stretching region. The deconvoluted peaks shaded in grey have a phase opposite to the non-shaded peaks. (Reprinted with permission from: Gopalakrishnan S, Jungwirth P, Tobias DJ, Allen HC. (2005) *J Phys Chem B* **109**(18): 8861–8872. Copyright 2005 American Chemical Society.)

the narrow peak at 3700 cm^{-1}: this is unambiguously attributed to dangling OH pointing towards the air–water interface. However, there is still a big controversy about the appropriate interpretation of the hydrogen bounded region of the spectra at 3000–3600 cm^{-1}. As a matter of fact, very different conclusions have been drawn based on the very same set of experimental data. The interpretation may even differ in qualitative aspects of the interfacial water structure.

First insights are gained by comparing the SFG surface spectra with the IR and Raman spectra of bulk water and hexagonal ice (Fig. 3). The bulk absorbance of hexagonal ice at 100 K shows a broad peak at 3200 cm^{-1} which is attributed to vibrational modes from the four oscillating dipoles associated with four-coordinate, hydrogen-bonded water molecules.[35] The absorbance of bulk water contains a broad peak centred at 3400 cm^{-1}.[36] Hence, the broad band observed in SFG spectrum resembles features of hexagonal ice and water.

Shen *et al.* introduced the term 'ice like band' to characterise the peak at 3200 cm^{-1}. This term is in a way misleading and needs some clarification. Scattering experiments reveal the complete absence of any long-range ice-like structural ordering within the surface layer of water. Instead, the term 'ice like' is meant to denote a highly dynamic surface of water forming a heavily distorted tetrahedral hydrogen bonding network

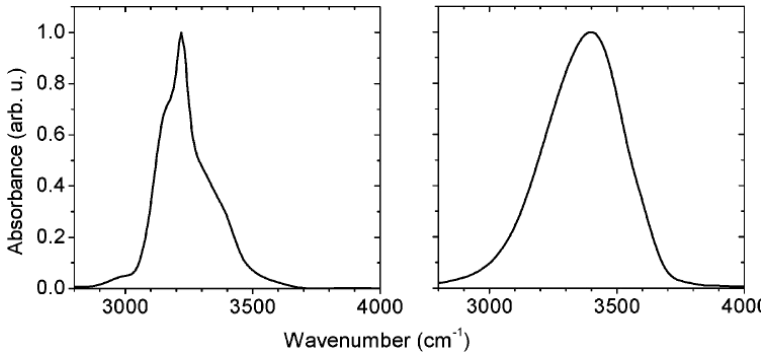

Fig. 3. Bulk absorbance of hexagonal ice at 100 K (left) and the bulk absorbance of liquid water (right). (Reprinted with permission from: Bettie JE, Labbe HJ, Whally E. (1969) *J Chem Phys* **50**: 4501; Querry MR, Wieliczka DM, Segelstein D. In *Handbook of Optical Constants of Solids II*, Academic Press: Boston, MA, 1991.)

of the hexagonal ice surface. The interfacial molecules are H-bonded to neighbours with dynamically varying strengths and geometries leading to fairly broad spectral feature (Fig. 4).

The previous section outlined the established fitting strategy for analysing the spectra and the underlying complexity. The non-linear resonant susceptibility is given by a summation of all individual resonances, which is then fitted to the spectral signature. However, the obtained fitting is not unique and there are different sets of resonances assigned to certain molecular arrangements that fully describe the experiment. As a consequence, the interfacial water architecture is interpreted in a different fashion and there is a controversial debate within the scientific community.[30,31,33,34,37–39]

Allen and Co-workers[40] attributed the 3200 cm^{-1} band to the vibrations of OH oscillators from surface water molecules that have one completely free OH (the 3700 cm^{-1} OH oscillator) and one OH that is hydrogen bonded to other water molecules (i.e. the other end of the free OH), the so-called DAA water molecules. This interpretation is supported by cluster studies.[41,42] Richmond's group[43,44] used molecular dynamics simulations to determine the population densities of different species of water molecules as functions of interfacial depth and orientation. The different configurations have been assigned different individual resonances and are used to reproduce the experiment. It is found that surface water molecules that possess one proton donor bond and one proton acceptor bond make the dominant contribution to both the *ssp*- and *sps*-polarised

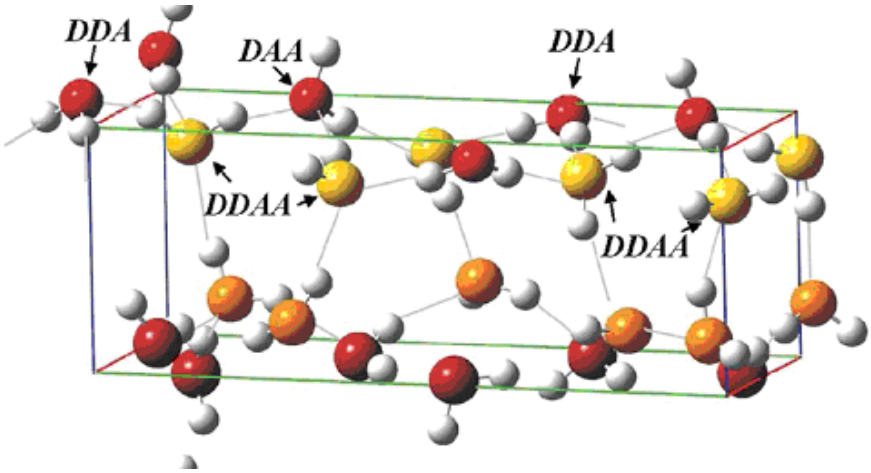

Fig. 4. Cartoons describing the structures of water vapour interfaces of neat water. The interfacial water structure is modelled after a distorted hexagonal ice. The top layer of the topmost layer (oxygen marked red) is occupied by DAA and DDA molecules, and the second layer (oxygen marked yellow) is occupied by DDAA molecules. Some DDAA molecules connecting to the molecules in the top layer with two donor bonds have an overall ice-like tetrahedral bonding structure. They contribute to the ice-like part of the vibrational spectrum. Other DDAA molecules are less symmetrically bonded to neighbours and contribute to the spectrum in the higher frequency region. The third and fourth layers (marked orange and red, respectively) have molecules with increasing randomness in position and orientation, closely resembling that of liquid water. (Reprinted with permission from Ref. 57. Copyright 2008 American Physical Society.)

spectral responses and are located within an Angstroem of the Gibbs dividing surface.

As a personal statement, we regard the assumption of discrete resonances in the water–air spectrum as inappropriate. The interface is highly dynamic. The continuous variations of hydrogen-bonding geometry and strength around interfacial water molecules shift and spread the OH stretching frequency into a highly inhomogeneously broadened band. The famous mathematician Neuman stated once, 'with four parameters I can fit an elephant, and with five I can make him wiggle his trunk.'[45] The assumption of too many individual resonances assigned to certain prevailing water configurations is a dead end for the description of a broad band spectrum with so few features.

Theoretical efforts to simulate the SFG spectra of water are able to reproduce the experimental features of the experiments. However, the

imaginary part of the susceptibility deduced from such studies differs with the recent phase-sensitive SFG experiments by Shen and co-workers. The aim of phase-sensitive measurements is the separate determination of the real and imaginary part of the non-linear susceptibility, instead of fitting the data to the square of the susceptibility. The measurement of amplitude and phase of the susceptibility tensor reduces the ambiguity in the interpretation of the SFG spectra. This is achieved by generating interference between a SFG signal generated in a material of known susceptibility, such as a quartz plate, and the one reflected from the water surface. The potential of phase-sensitive measurement has been recognised early but it remains a time-consuming and challenging experiment.[46]

Shen and Ostroverkhov performed phase-sensitive measurements of the air–water interface in a further developed experimental setup using a quartz reference plate and a phase modulator (Fig. 5).[47,48] In particular, by directly measuring the imaginary component of the non-linear

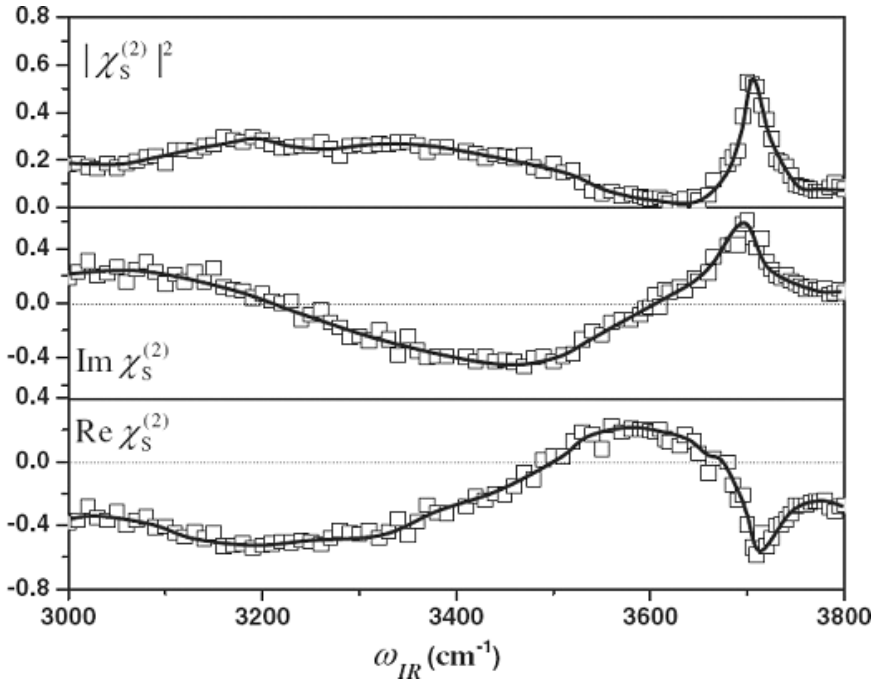

Fig. 5. Spectra of $|\chi_S^{(2)}|^2$, $\mathrm{Im}\chi_S^{(2)}$, and $\mathrm{Re}\chi_S^{(2)}$ for the neat water vapour interface in the OH stretching range obtained with phase sensitive sum frequency spectroscopy. (Reprinted with permission from Ref. 57. Copyright 2008 American Physical Society.)

susceptibility in the water region, they found that the lower frequency component ($< 3200\,\mathrm{cm}^{-1}$) is in phase with that of free OH, while the mid-frequency component (3200–$3600\,\mathrm{cm}^{-1}$) is out of phase. In their model, the loosely coined ice-like and liquid-like features are further refined and their contribution to the interfacial spectrum of water has been reported. This is in contradiction to the above mentioned theoretical modelling which assumes that both the ice-like and liquid-like bands are opposite in sign with respect to the dangling OH peak.

Recently, an alternative assignment of the modes has been put forward for the surface vibrational spectrum of water. The focus is again on the band which occurs between 3000–$3600\,\mathrm{cm}^{-1}$ where the vibrational coupling (intramolecular) between the stretch and the bending overtone contribution to the spectrum has been suggested instead of structural effects.[49]

SFG spectroscopy is usually used to study the static properties of aqueous interfaces. The use of a pump-probe geometry can additionally allow detection of time-resolved SFG spectra.[50–54] This permits the study of ultrafast vibrational dynamics of neat water interfaces. Measurements on interfacial bonded OH stretching modes revealed relaxation behaviour on sub-ps time scales in close resemblance to that of bulk water.[54] Vibrational excitation is followed by spectral diffusion, vibrational relaxation, and thermalisation in the hydrogen-bonding network. Bonn and co-workers used femtosecond time–resolved SFG spectroscopy to study the OH stretching vibrational lifetime of hydrogen-bonded interfacial water. The vibrational lifetime in the frequency range of 3200 to $3500\,\mathrm{cm}^{-1}$ is found to closely resemble that of bulk water, indicating ultrafast exchange of vibrational energy between surface water molecules and those in the bulk. Bonn also studied the vibrational coupling of water molecules adjacent to a lipid membrane.[50] Interestingly, they show that membrane-bound water is physically removed from the bulk, and the energy transfer resulting from dipolar interactions between the surface and bulk is not as efficient as for the neat air–water interface, indicating that water is an intrinsic part of the lipid membrane.

In short, the story of the interpretation of the water surface is still under debate and requires further refinement.

3.4. *Ions at the Air–Water Interface*

As outlined in the introduction, MD simulations predict a non-monotonous concentration profile for large and polarisable anions at the

air–water interface in contrast to the established textbook picture which suggests a surface depleted of ions. However, up till now the direct measurement of this ion profile remains an unsolved experimental challenge. Most of the evidence is based on non-linear optical techniques covered in this section and on X-ray scattering techniques as well as on X-ray fluorescence which are discussed in Chap. 5.

SFG spectroscopy has been used to study the influence of the ions on the interfacial water structure. These measurements are indirect; it is not the salt that is studied but the impact of the ions on the local water environment. Two groups investigated a series of aqueous sodium halogenide salt solutions in a systematic fashion to analyse the impact of the anion on the interfacial water structure. The spectra reveal profound changes with respect to the neat water surface and are shown in Fig. 6. The SFG spectra of 2-M NaI solution showed a significant enhancement of the liquid-like band and the appearance of a broad shoulder above the dangling OH peak as compared to the neat air–water SFG spectrum.

Based on this data set, Allen and co-workers[33] concluded a confirmation of the MD simulation results on the enhanced adsorption of the more polarisable anions within the interfacial region. The observed spectral changes were attributed to I^- ions disrupting the interfacial H-bonding network and creating more asymmetrically H-bonded molecules. Furthermore, a comparison of the intensity changes in the SFG spectra with the corresponding bulk IR and Raman spectra in the 3000–3600 cm^{-1} region was interpreted as an increase of the effective interfacial layer thickness, providing corroborative evidence for the MD predictions. Richmond and co-workers challenged this point of view. According to their interpretation, the observed changes in the SFG spectra do not necessarily indicate the increase of the thickness of the surface water layers at the electrolyte solution surfaces. Instead, the observed changes of the spectrum can also be attributed to a blue shift and a narrowing of the mode at $\sim 3400\,cm^{-1}$ with no significant changes in the mode strengths of bonded OH.[39]

As expected, NaI showed the most profound effect on the interfacial water structure; the impact of the other salts followed the order given in the periodic table. The intensity of the hydrogen-bonded water in the broad 3400 cm^{-1} band increased in the order of NaCl, NaBr, and NaI; while the intensity of the broad band around 3250 cm^{-1} decreased with the same order. The SFG spectra of the NaF aqueous solution surface measured in Allen and Richmond laboratory did not agree in the 3000–3600 cm^{-1}

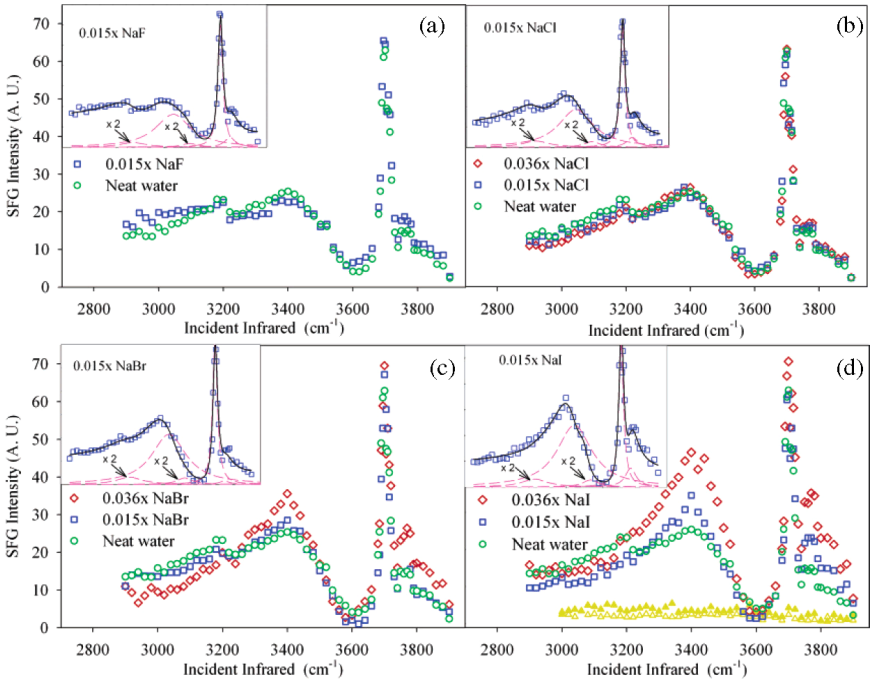

Fig. 6. SSP polarised SFG spectra of (a) 0.015× NaF, (b) 0.015× and 0.036× NaCl, (c) 0.015× and 0.036× NaBr, and (d) 0.015× and 0.036× NaI. The neat water SFG spectrum is plotted in each figure for comparison. The open yellow and closed yellow triangles within (d) show the sum frequency intensity of the 0.015× NaI in D2O and pure D2O, respectively. Insets: SFG sodium halide aqueous solutions spectral fits. Component Lorentzian peaks are shown as dashed pink lines, and the calculated fits from the component peaks are shown as black lines that go through most of the data points. (Reprinted with permission from: Liu D, Ma G, Levering LM, Allen HC. (2004) *J. Phys. Chem. B* **108**: 2252. Copyright 2004 American Chemical Society.)

spectral region, while the 3700 cm^{-1} remained almost unchanged from that of the neat air–water interface.

The differences may be due to impurities within the sample. Surface active impurities are a major concern in these studies. It turns out that salts purchased with a claimed purity of 99.999% may contain traces of organic surface active components. These impurities do not play any role for investigations of bulk properties; however, they are extremely disturbing for the investigation of interfacial properties. To underline the importance of the purification of salts, our group[55] compared the SFG spectra

of the as purchased salt from Sigma–Aldrich claimed to be of purity in the third decimal places with that of the specially purified salt solution. The organic contaminants show up directly in the SFG spectra around 2800–3000 cm^{-1} region. Further the free OH intensity around 3700 cm^{-1} is considerably lowered and the broad region around 3000–3600 cm^{-1} is significantly modified. Hence, as good code of conduct we suggest to extend the presentation of the interfacial water SFG spectra to the spectral range of 2800–3000 cm^{-1} for instance as an inset. Surface active impurities would leave the spectral signature of the hydrocarbon chains. Hence, the absence of any peaks in this region is absolutely convincing for monitoring the desired purity and it is more sensitive than a discussion based on the 3700 cm^{-1} OH peak.

Shen and co-workers[56,57] employed the phase-sensitive SFG-VS measurement and studied the *ssp* SFG-VS spectra of the NaI aqueous solution surfaces in comparison with the neat air–water interface. The authors concluded that the presence of I^- anion near the interface region may not disturb the water molecular structure at the topmost surface layer, while it can reorientate the water molecules in the subphase. Their data confirmed the influence of the interfacial water hydrogen bonding structure by the I^- anions of the previous SFG studies.

In a recent study, the influence of indifferent electrolytes on the adsorption behaviour of cationic soluble surfactant solutions has been investigated by surface tension measurements, ellipsometry and surface second harmonic generation (SHG).[58–60] Each technique addresses different structural aspects and the combined data provide a detailed picture of the interfacial architecture. The analysis gives an indirect proof of the existence of a phase transition between the free and condensed state of the counterions caused by a small increase of surface charge close to the critical micelle concentration (cmc).

In addition, SFG spectroscopy can be used to indirectly detect ion distributions at charged interfaces using water vibrational signatures.[58–61] The strength of the SFG response depends on the number of oriented water molecules. At a charged aqueous interface, the electric field at the surface aligns the polar water molecules, which in turn increases the SFG response. This enhancement of the water vibrational signal can be used to indirectly detect the depth of the electric field in the solution, which consequently depends on the ion distribution in the vicinity of the interface.

In Ref. 60, the surface charge itself was tuned by the amount of adsorbed ionic surfactants (1-dodecyl-4-dimethylaminopyridinium bromide — DMPB[58]). Charging up the interface by a small amount of DMP leads to an increase in SF intensity by a factor of ten. A further increase of the surface charge leads to stronger electric fields at the interface, however, the charge will also be more effectively screened by the counterions. This leads to an overall decreased depth of the electric field, which goes along with a decreased amount of oriented water molecules at the interface. Less oriented water molecules reduce the SFG response which was observed in the experiments.

The enhancement of the electric field by about a factor of ten is not specifically related to the surfactant used, as it is also observed in the context of charged lipid monolayers at the air–water interface. Wurpel and co-workers used λ-phage DNA bound to a cationic lipid monolayer at the air–water interface to study screening effects of counterions by detecting water signals in the OD stretching region at different concentrations.[61]

Further studies in this direction may also involve solid surfaces of different surface chemistry which can be used as electrodes to change the surface potentials in a fast and controlled manner. Diamond for example has a large electrochemical potential window, making this material particularly suitable for studying ion distributions.[62] The comparably flat surface of diamond (roughness in the nm regime) can also be functionalised to obey a hydrophilic or hydrophobic surface (hydrogen or oxygen terminated).

The SFG measurements applied in all these studies are indirect. Not the ion is monitored but instead the impact of the presence of ions in the interface on the water structure. In this way the studies of Viswanath and Motschmann[63,64] are unique. The extreme candidate of the Hofmeister series of ions, thiocyanate, was studied at the air–water interface using SFG spectroscopy. The stretching vibration of the ion is monitored and polarisation-dependent measurements have been used to retrieve the orientation of the ion. Secondly, the impact of the ion on the interfacial water is studied, allowing a correlation of the perturbation of solvent features due to the presence of ions at the interface. Figure 7 shows the CN vibrational stretch of the thiocyanate anion in all polarisation combinations around 2064 cm^{-1}, confirming its enrichment at the interface. This rod-like anion adopts a preferential orientation in the order of 45 degrees with respect to the normal to the surface. The presence of the SCN^- ion at the interface leads to a decrease of 3200 cm^{-1} and a slight increase of 3400 cm^{-1} bands.

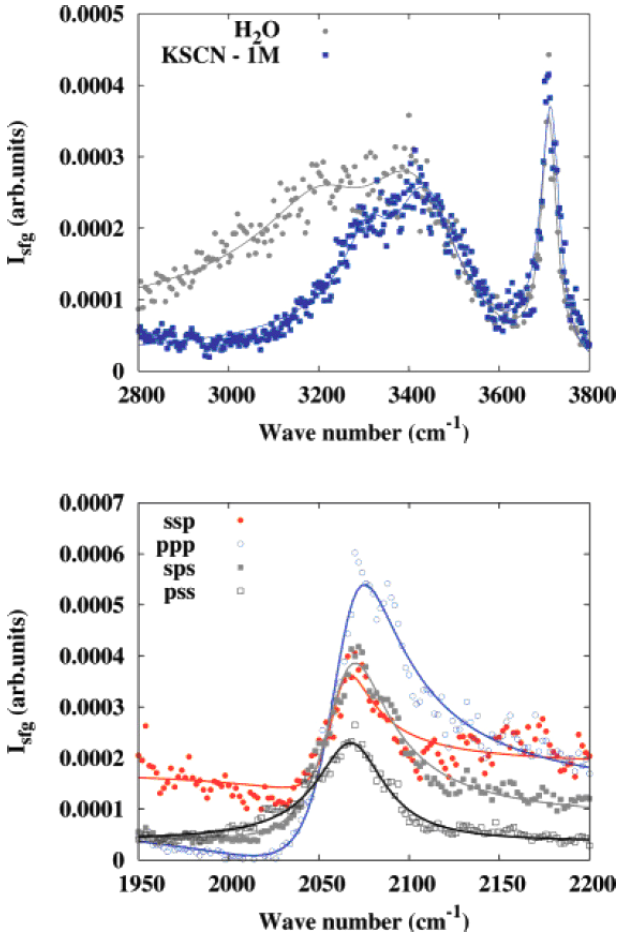

Fig. 7. Vibrational sum frequency spectra of water and ∼ 1 M potassium thiocyanate solution. The presence of the ions at the interface decreases the 3200 cm^{-1} band. The presence of the ion has also been directly monitored by observing the CN stretch of thiocyanate anion for ∼ 1 M potassium thiocyanate solution. The points and continuous lines represent the experimental data and fits, respectively. (Reprinted with permission from Refs. 63 and 64. Copyright 2007 and 2008 American Chemical Society.)

The combined data are a convincing piece of evidence for the interfacial propensity of the ion to adsorb at the interface. This study demonstrates the applicability of the SFG technique on air–electrolyte solutions to probe directly the presence of an oriented anion in addition to its implications on interfacial water signature. Furthermore, this work shows that

the orientation of the anion is relevant and needs to be taken into account to get a full picture on the interfacial architecture.

As evident from the previous section, the spectral assignment of interfacial water is still an intense area of research with some controversy. Surface water molecules with different hydrogen bonding structures exhibit different vibrational spectral features. This is a strength but also the burden of SFG. The spectral features of the interfacial water spectrum are fairly broad, leading to an ambiguity in the fitting procedure. Hence, the conclusions drawn from the interpretation of the spectra are model dependent. Due to the importance of the understanding of water at interfaces, we expected a significant progress in the interpretation of surface SFG data. The review article of Wang and colleagues[65] discusses possible alternative descriptions based on a microscopic theory using an induced dipole lattice which eliminates some of the critical issues. Nevertheless, despite some controversial model dependent elements, SFG spectroscopy yields a mounting evidence for the interfacial propensity of large and polarisable ions at the air–water interface.

SHG is a related non-linear technique that also provides valuable insight in the interfacial architecture. SHG is determined by the electronic states of the molecules and as a consequence it is not as much influenced by the subtle details of the interface. Hence, the interpretation of the experimental data is simpler and more robust. A major remaining concern is the impossibility to separate quadrupolar contributions generated in the bulk phase from the surface contribution to the total SHG signal. Here some assumptions are introduced which may be challenged.[66]

SHG can be applied in two fashions in a resonant mode and a non-resonant mode. The non-resonant SHG signal measures the whole water surface layer without any discrimination on the surface water molecules in different hydrogen-bonding configurations. Therefore, non-resonant SHG is an appropriate tool to estimate the number of oriented molecules contributing to the SHG signal in a semi-quantitative fashion. The SHG response is governed by the number density and the orientational distribution of the molecules.[67] A careful polarisation-dependent measurement allows separation of both contributions.[68] The SHG intensity allows then an estimation of the relative increase of the average thickness of the total surface water.

Wang and co-workers[69,70] performed polarisation-dependent SHG measurements from the interfacial water molecules of the NaF, NaCl, and

NaBr aqueous electrolyte solutions. The quantitative polarisation analysis of the measured SHG data showed that the average orientation of the interfacial water molecules changed slightly with the bulk concentration of the NaF, NaCl and NaBr salts as compared to the neat air–water interface. The increase in the SHG signal with the bulk salt concentration was attributed to an increase of the thickness of the interfacial water molecular layer. The average thickness of the surface water layers increased with the bulk electrolyte concentration in an almost linear fashion in the following order: KBr > NaBr > KCl > NaCl $\cong$ NaF. The change of the average thickness of the surface water layers was less than 35% as compared to the neat air–water interface, even at very high salt concentration up to five molar solutions for the NaBr and four molar solution for the KBr. The absence of the electric-field–induced SHG (EFISHG) effect indicated further that the electric double layer at the salt aqueous solution surface is weaker as expected from molecular dynamics (MD) simulations.[71]

A second alternative to apply SHG is to use it in a resonant mode which enables direct monitoring of selected ions. Saykally *et al.* investigated the surfaces of electrolyte solution using resonant SHG. These experiments utilise the charge-transfer-to-solvent (CTTS) transitions in the UV and enabled direct monitoring of the anion. CTTS transitions exhibit very large non-linear cross sections as the direct consequence of the charge separation that is associated with the transition. By measuring the SHG intensity on and off resonance with the anions, the total SHG intensity can be separated into the contributions from the anions and the water background, and the surface concentration of the anions can be extracted. Several ions fulfil these prerequisites — e.g. iodide (I^-),[72] ferrocyanide [$Fe(CN)_6^{4-}$],[73] azide (N^{3-}),[74] and thiocyanate (SCN^-)[75] — and have been studied by resonant SHG (see Fig. 8). In the same spectral region, the water hyperpolarisability is non-resonant and contributes to the signal via its concentration-dependent non-resonant susceptibility term.

These data also provide a strong proof for the presence of the polarisable ions at the interface. Due to the relatively small hyperpolarisability of iodide, it is still not possible to determine whether the iodide anions are enhanced at the interface or whether the surface mole fraction increases linearly with the bulk.

In the last decade, tremendous progress has been made theoretically and experimentally in understanding the distribution of aqueous ions at the charged and uncharged interface. Among other experimental techniques,

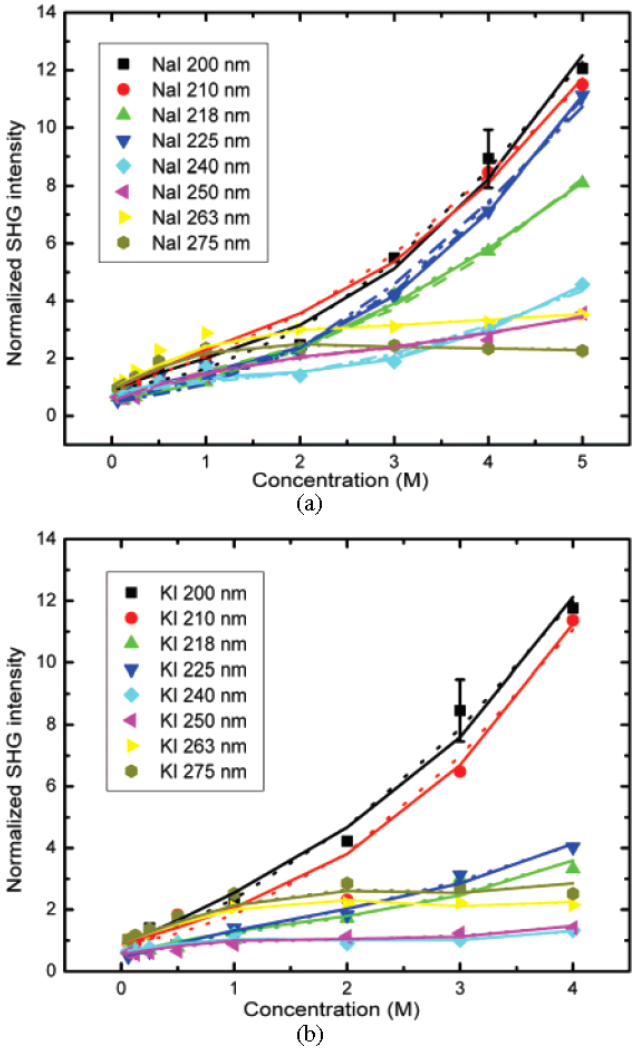

Fig. 8. Resonant SHG of NaJ and KJ. The high concentration increase in the resonant SHG intensity is due to iodide anions at the interface forming a dense ionic double layer with the cations. Due to the relatively small hyperpolarisability of iodide, it is not possible to determine whether the iodide anions are enhanced at the interface or whether the surface mole fraction increases linearly with the bulk. (Reprinted with permission from Ref. 76. Copyright 2006 American Physical Society.)

linear and non-linear optical methods can be applied under normal conditions and the only requirement is that the sample can be reached by light. In addition, spectroscopy methods can distinguish between several molecular species present at the interface. Water can be used as a probe to study ion distributions at charged solid or liquid interfaces. More complex ions with vibrational signatures can directly be detected and orientational distributions can be determined with the aid of polarised laser light sources. In a further approach, these interfaces may be designed to be more complex. In a systematically manner, for example, simple biomolecules under changing surface chemistry in different environmental conditions can be studied in various spectral regions related to the biomolecule, water and/or complex ions. Furthermore, with the aid of time-resolved SFG spectroscopy, the dynamics of water molecules and the energy exchange to bulk water molecules at charged or uncharged interfaces can be studied. Overall, optical techniques provide the experimental tools to get molecular level-based information needed to further our understanding of ions at interfaces.

References

1. McDevit *et al.* (1952) *J Am Chem Soc* **74**: 1773.
2. Wyman JT, Edsall J. (1951) *Biophysical Chemistry*. Academic Press.
3. Pinna MC, Salis A, Monduzzi M, Ninham BW. (2005) *J Phys Chem B* **109**: 5406–5408.
4. Jungwirth P, Tobias DJ. (2006) *Chem Rev* **106**: 1259–1281.
5. Smith D, Saykally RJ, Geissler PL. (2007) *J Am Chem Soc* **129**: 13847.
6. Mancinelli R, Botti A, Bruni F, Ricci MA, Soper AK. (2007) *J Phys Chem B* **109**: 13570.
7. Collins KD. (2004) *Methods* **34**: 300–311.
8. Jarvis and Scheiman. (1968) *J Phys Chem* **72**: 74.
9. Pugh R. (1996) *Journal of Colloid and Interface Science* **184**: 550–563.
10. Onsager L, Samaras NNT. (1934) *J Chem Phys* **2**: 528.
11. Gopalakrishnan S, Liu DF, Allen HC, Kuo M, Shultz MJ. (2006) *Chem Rev* **106**: 1115.
12. Tobias DJ, Hemminger JC. (2008) *Science* **319**: 1197.
13. Bloembergen N, Pershan PS. (1962) *Phys Rev* **128**: 606.
14. Du Q, Superfine R, Freysz E, Shen YR. (1993) *Phys Rev Lett* **70**: 2313.
15. Heinz TF, Divincenzo DP. (1990) *Phys Rev A* **42**: 6249.
16. Zhu XD, Shen YR. (1990) *Phys Rev A* **41**: 4549.
17. Andrews DL, Blake NP. (1990) *Phys Rev A* **41**: 4550.
18. Shen YR. (1999) *Appl Phys B* **68**: 295.
19. Wei X, Hong SC, Lvovsky AI, Held H, Shen YR. (2000) *J Phys Chem B* **104**: 3349.

20. Held H, Lvovsky IA, Wei X, Shen YR, (2002) *Phys Rev B* **66**: 205110.
21. Boyd RW. (1992) *Non-linear Optics*. Academic Press, San Diego.
22. Hirose C, Akamatsu N, Domen K. (1992) *Appl Spectr* **46**: 1051–1072.
23. Born M, Wolf E. (1999) *Principles of Optics: Electromagnetic Theory of Propagation, Interference and Diffraction of Light (Paperback)*. Cambridge University Press.
24. Motschmann H, Penner T, Armstrong N, Enzenyilimba M. (1993) *J Phys Chem* **97**: 3933.
25. Hommel EL, Ma G, Allen HC. (2001) *Analytical Sciences* **17**(11): 1325–1329.
26. Hommel EL, Allen HC. (2001) *Analytical Sciences* **17**(1): 137–139.
27. Richter LJ, Petralli-Mallow TP, Stephenson JC. (1998) *Opt Lett* **23**(20): 1594–1596.
28. Ishibashi T, Onishi H. (2001) *Chemical Physics Letters* **346**(5–6): 413–418.
29. vanderHam EWM, Vrehen QHF, Eliel ER (1996). *Optics Letters* **21**(18): 1448–1450.
30. Wei X, Shen YR. (2001) *Phys Rev Lett* **86**: 4799.
31. Gragson DE, McCarty BM, Richmond GL. (1996) *J Phys Chem* **100**: 14272.
32. Baldelli S, Schnitzer C, Shultz MJ, Campbel DJ. (1997) *J Phys Chem B* **101**: 10435.
33. Liu D, Ma G, Levering LM, Allen HC. (2004) *J Phys Chem B* **108**: 2252.
34. Gan W, Wu D, Zhang Z, Feng R, Wang H. (2006) *J Chem Phys* **124**: 114705.
35. Bertie JE, Labbe HJ, Whally E. (1969) *J Chem Phys* **50**: 4501.
36. Querry MR, Wieliczka DM, Segelstein D. (1991) In *Handbook of Optical Constants of Solids II*. Academic Press, Boston, MA.
37. Brown MG, Raymond EA, Allen HC, Scatena LF, Richmond GL. (2000) *J Phys Chem A* **104**: 10220.
38. Raymond EA, Tarbuck TL, Richmond GL. (2002) *J Phys Chem B* **106**: 2817.
39. Raymond EA, Richmond GL. (2004) *J Phys Chem B* **108**: 5051.
40. Gopalakrishnan S, Jungwirth P, Tobias DJ, Allen HC. (2005) *J Phys Chem* **109**: 8861.
41. Devlin JP, Sadlej J, Buch V. (2001) *J Phys Chem A* **105**: 974.
42. Steinbach C, Andersson P, Kazimirski JK, Buck U. (2004) *J Phys Chem A* **108**: 6165.
43. Walker DS, Hore DK, Richmond GL. (2006) *J Phys Chem B* **110**: 20451–20459.
44. Walker DS, Richmond GL. (2008) *J Phys Chem C* **112**: 201–209.
45. Dyson F. (2004) *Nature* **427**: 297.
46. Ong TH, Davies PB, Bain CD. (1993) *J Phys Chem* **97**: 12047–12050.
47. Ji N, Ostroverkhov V, Tian CS, Shen YR. (2008) *Phys Rev Lett* **100**: 096102.
48. Tian CS, Shen YR. (2009) *J Am Chem Soc* **131**: 2790–2791.
49. Sovago M, Campen RK, Wurpel GWH, Muller M, Bakker HJ, Bonn M. (2008) *Phys Rev Lett* **100**: 173901.
50. Bredenbeck J, Ghosh A, Smits M, Bonn M. (2008) *J Am Chem Soc* **130**: 2152–2153.
51. Smits M, Ghosh A, Sterrer M, Muller M, Bonn M. (2007) *Phys Rev Lett* **98**: 098302.
52. Hayashi M, Shiu YJ, Liang KK, Lin SH, Shen YR. (2007) *J Phys Chem A* **111**: 9062–9069.

53. Backus EH, Grecea ML, Kleyn AW, Bonn M. (2007) *J Phys Chem B* **111**: 6141–6145.
54. McGuire JA, Shen YR. (2006) *Science* **313**: 1945–1948.
55. Koelsch P, Viswanath P, Motschmann H, Shapovalov VL, Brezesinski G, Moehwald H *et al.* (2007) *Colloids & Surfaces A-Physicochemical & Engineering Aspects* **303**: 110.
56. Tian CS, Ji N, Waychunas GA, Shen YR. (2008) *J Am Chem Soc* **130**: 13033.
57. Ji N, Ostroverkhov V, Tian CS, Shen YR. (2008) *Phys Rev Lett* **100**: 096102.
58. Koelsch P, Motschmann H. (2005) *Langmuir* **21**(8): 3436–3442.
59. Koelsch P, Motschmann H. (2004) *Current Opinion in Colloid & Interface Science* **9**(1–2): 87–91.
60. Koelsch P, Motschmann H. (2004) *J Phys Chem B* **108**(48): 18659–18664.
61. Wurpel GWH, Sovago M, Bonn M. (2007) *J Am Chem Soc* **129**(27): 8420.
62. Hartl A, Schmich E, Garrido JA, Hernando J, Catharino SCR, Walter S, Feulner P, Kromka A, Steinmuller D, Stutzmann M. (2004) *Nat Mater* **3**(10): 736–742.
63. Viswanath P, Motschmann H. (2007) *J Phys Chem C* **111**(12): 4484.
64. Viswanath P, Motschmann H. (2008) *J Phys Chem C* **112**(6): 2099.
65. Zheng DS, Wang Y, Liu AA, Wang HF. (2008) *International Reviews in Physical Chemistry* **27**: 629–664.
66. Andrews DL. (1993) *J Mod Opt* **40**: 939.
67. Simpson GJ, Rowlen KL. (2000) *Anal Chem* **72**: 3399.
68. Simpson GJ, Rowlen KL. (2000) *Anal Chem* **72**: 3407.
69. Bian HT, Feng RR, Xu YY, Guo Y, Wang HF. (2008) *Phys Chem Chem Phys* **10**: 4920.
70. Zhang WK, Wang HF, Zheng DS. (2006) *Phys Chem Chem Phys* **8**: 4041.
71. Brown MA, D'Auria R, Kuo I-FW, Krisch MJ, Starr DE, Bluhm H, Tobias DJ, Hemminger JC. (2008) *Phys Chem Chem Phys* **10**: 4778.
72. Petersen PB, Johnson JC, Knutsen KP, Saykally RJ. (2004) *Chem Phys Lett* **397**: 46–50.
73. Petersen PB, Saykally RJ. (2005) *J Am Chem Soc* **127**: 15446–15452.
74. Petersen PB, Saykally RJ. (2004) *Chem Phys Lett* **397**: 51–55.
75. Petersen PB, Saykally RJ, Mucha M, Jungwirth P. (2005) *J Phys Chem B* **109**: 10915–10921.
76. Petersen PB, Saykally RJ. (2006) *J Phys Chem B* **110**: 14060–14073.